Critically-stressed reservoir stimulation direction via stress preconditioning in horizontal EGS doublets

Barnaby Fryer[1], Xiaodong Ma[2], Gunter Siddiqi[3], and Lyesse Laloui[1]

[1]Ecole Polytechnique Fédérale de Lausanne
[2]ETH Zürich
[3]Swiss Federal Office of Energy

November 21, 2022

Abstract

In this work, it is suggested numerically that it is possible to direct shear stimulation treatments in critically-stressed reservoirs. This would aid in the creation of Enhanced Geothermal Systems by promoting hydraulic connectivity in doublet-well systems. In this case, the stimulation treatment is directed using only the poroelastic stress changes associated with a previous stimulation treatment to precondition the stress field. This methodology is shown for reverse, strike-slip, and normal faulting stress regimes.

Geothermics manuscript No.
(will be inserted by the editor)

Critically-stressed reservoir stimulation direction via stress preconditioning in horizontal EGS doublets

Barnaby Fryer[a,1] · **Xiaodong Ma**[b] ·
Gunter Siddiqi[c] · **Lyesse Laloui**[a]

Received: date / Accepted: date

Abstract In this work, it is suggested numerically that it is possible to direct shear stimulation treatments in critically-stressed reservoirs. This would aid in the creation of Enhanced Geothermal Systems by promoting hydraulic connectivity in doublet-well systems. In this case, the stimulation treatment is directed using only the poroelastic stress changes associated with a previous stimulation treatment to precondition the stress field. This methodology is shown for reverse, strike-slip, and normal faulting stress regimes.

Keywords EGS · Reservoir Stimulation · Reservoir Engineering · Poroelastic stress · Hydraulic Shearing

Highlights

1. It is suggested that shear stimulation treatments in EGS reservoirs can be directed
2. Injection-induced poroelastic stress changes are significant in a critically-stressed crust
3. The methodology is shown for reverse, strike-slip, and normal faulting stress regimes

[a]Laboratory of Soil Mechanics, École Polytechnique Fédérale de Lausanne, Lausanne, Switzerland
[b] ETH Zürich, Swiss Competence Center for Energy Research - Supply of Electricity (SCCER-SoE) and Chair for Geothermal Energy and Geofluids
[c] Swiss Federal Office of Energy, Bern, Switzerland
[1] **Corresponding Author:** B. Fryer E-mail: barnaby.fryer@epfl.ch

1 Introduction

Low permeability and inter-well connectivity are common problems preventing Enhanced Geothermal Systems (EGS) from reaching their potential (Tester et al., 2006; Ziagos et al., 2013). Indeed, it has previously been pointed out that the optimal distribution of permeable pathways is critical for the successful development of sufficient productivity for commercial EGS power generation (Robinson et al., 1971; Ziagos et al., 2013). For this reason, the ability to guide reservoir stimulation treatments such that specific areas of the reservoir can be targeted for stimulation would represent a significant development. A further advantage of this kind of stimulation targeting would be the ability to avoid the reactivation of large faults; either directly in the case that fault locations are known, or indirectly, in that only the most crucial parts of a reservoir are stimulated, thus moderating the risk that the stimulation treatment encounters large faults (e.g., Kim et al. (2018)). This should aid in the mitigation of induced seismicity. In fact, it is thought that the development of alternate stimulation concepts is integral to the mitigation of seismic risk from hydraulic stimulation (Häring et al., 2008) and that the engineering of reservoir connectivity would represent a key development for EGS (Rybach, 2010).

Directed reservoir stimulation techniques have been investigated before. For example, in Soultz-sous-Forêts, Baria et al. (2004) showed the positive effect of the contemporaneous stimulation of two wells in the context of an EGS project in crystalline rock. Their focus was primarily on the effect that an elevated pore pressure would have on the stimulation of a second well. However, the idea of altering the stress field in order to benefit a stimulation treatment has also been suggested as long ago as 1977 when Shuck (1977) filed a patent which involved injecting fluid to alter the plane of the maximum principal stress for use in hydraulic fracturing. Boutéca et al. (1983) investigated, both numerically and experimentally, the possibility of using fluid injection to alter the stress state such that a hydraulic fracturing treatment would connect two wells. This idea has been expanded upon by, for example, Warpinski and Branagan (1989), who were able to show stress changes of over 2 MPa due to the opening of a hydraulic fracture in lenticular reservoirs with the intent of reorienting potential hydraulic fractures such that they would intersect natural ones. Warpinski and Branagan (1989) estimated that larger pre-stimulation treatments would be able to induce stress changes of over 4 MPa, which, in this case, was a stress change large enough to swap the directions of the principal horizontal stresses. Warpinski and Branagan (1989) primarily considered their results relevant for single-well systems. Certainly, the effect of stress shadowing due to fracture opening has been widely discussed (e.g., Fisher et al. (2004); Vermylen and Zoback (2011)). Other relevant works include the effects of fluid-production-induced poroelastic stress changes on refracturing (Elbel and Mack, 1993), the work by Minner et al. (2002), which showed that injection and production can result in poroelastic stress changes that can dramatically alter fracture geometry on infill wells, and Berchenko and Detournay (1997); Gao et al. (2019) who used models to analyze the deviation of hydraulic fractures associated with poroelastic stress changes resulting from production and injection.

Although there have been a number examples of EGS in sedimentary rocks (e.g., Evans et al. (2012)), the focus here will be on EGS in crystalline rocks, which tend to be deeper and therefore typically offer higher temperatures. Various configurations exist for EGS wells (e.g., Chen and Jiang (2015)), but a typical EGS setup might employ a doublet well configuration (e.g., Jupe et al. (1992); Dorbath et al. (2009); Kim et al. (2018)) whereby fluid is circulated between an injection and a production well, where these wells can either be vertical or directional in nature. Crystalline rock and high temperatures do pose new challenges for directional drilling, but improvements are being made. Certainly, a number of EGS wells have been drilled directionally (e.g., Tester et al. (2006); Kwiatek et al. (2008); Dorbath et al. (2009); Kwiatek et al. (2014); Kim et al. (2018); Norbeck et al. (2018); Kwiatek et al. (2019)) and horizontally drilling in hard, high temperature rock is possible (albeit potentially cost inhibitive) (Shiozawa and McClure, 2014). In fact, recent publications are beginning to consider the multi-stage stimulation of horizontal wells for EGS (e.g., Meier et al. (2015); Kumar and Ghassemi (2019)). It has even been suggested that the multi-stage horizontal well stimulation employed in the oil and gas industry should act as a model for the EGS industry (Ziagos et al., 2013; U.S. Department of Energy, 2019).

Typically, for EGS in crystalline rock, the reservoirs are primarily thought to be stimulated in shear (Evans et al., 2005b; Zang et al., 2014). Coulomb faulting theory is a typical way to assess shear failure potential. From Coulomb faulting theory, it is clear that an increase in pore pressure reduces the effective stress on a shear plane and brings the shear plane closer to failure. Indeed, in many instances of shear stimulation in crystalline rock, it is thought that the increase in pore pressure was the dominant contributor to the induced shear displacement (Pearson, 1981; Pine and Batchelor, 1984; Jupe et al., 1992; Deichmann and Giardini, 2009). From Coulomb faulting theory it is clear that it is possible to stimulate EGS reservoirs with injection pressures below the minimum principal stress. This is a fundamental difference between EGS stimulation and hydraulic fracturing operations, as hydraulic fracturing operations occur at injection pressures above the minimum principal stress in order open fractures in a tensile manner. However, changes in total stress can also cause shear failure. For example, poroelastic stress changes, or the stress changes resulting from pore pressure-induced deformation of reservoir rock, have been shown to be significant in induced seismicity, where they have at times been largely responsible for fluid production (e.g., Segall (1989)), injection (e.g., Chen et al. (2017)), and hydraulic fracturing (e.g., Deng et al. (2016)) operation-induced seismicity. Poroelastic stressing differs from changes in pore pressure in that it does not necessarily lead to isotropic changes in effective stress. A simple increase or decrease in pore pressure will not directly lead to a change in the differential stress; however, importantly, the resulting poroelastic changes to total stress can be, and frequently are, anisotropic.

This induced anisotropy allows poroelastic stress changes to have a significant influence on a shear plane's potential for failure, even when small in magnitude, as these changes are capable of either increasing or decreasing differential stress.

In this work, the stimulation of an EGS doublet well system will be investigated. Specifically, an investigation will be made into the possibility of guiding the stimulation from one well to another, as previously discussed by Baria et al. (2004). Unlike in Baria et al. (2004), however, this work will consider poroelastic stress changes, which have been shown to be relevant in EGS stimulations (Jacquey et al., 2018), as well as address the three main stress regimes in generic scenarios. This investigation will be carried out by first stimulating one of the doublet wells according to normal stimulation procedure. The stress changes associated with this first stimulation treatment will then encourage stimulation in a certain direction, allowing the stimulation treatment of the second well to be guided toward the stimulated region surrounding the first well. In this way the stress field is "preconditioned" before the stimulation of the second well. The advantage of this methodology is that it (1) helps ensure connectivity between the two doublet wells and (2) reduces the stimulation of less useful rock mass, which decreases the chance of accidentally inducing a large magnitude event on a nearby fault. This investigation will be performed with a poroelastic reservoir simulator where the permeability enhancement is based on the results of field studies. Even if, as mentioned above, further technological advancement may be necessary to allow horizontal EGS wells to be readily and cost-effectively drilled, here the investigation will concern the stimulation of horizontal EGS doublet wells drilled in critically-stressed crystalline rock. This investigation will also have implications for directionally-drilled wells; however, in these cases the results would depend on the inclination of the wells. Although significant temperature differences may typically be present between the injected fluid and reservoir during EGS stimulations, the analysis here will be isothermal to isolate the effects of poroelasticity.

2 Methodology

In order to model the pressure and stress changes resulting from either fluid production or injection, a sequentially coupled 2-D plane strain poroelastic reservoir simulator is employed. Although the model is 2-D plane strain, it will be appropriate for modelling 3-D stress changes due to fluid production and injection activities from horizontal wells which are parallel to a principal stress direction (Cheng, 2016). An equivalent continuum approach will be employed, meaning that fractures will not be explicitly modelled, a previously explored approach for modelling fractured media (e.g., Oda (1986); Miller (2015); Gan and Elsworth (2016)). This approach was taken because the fractured rock mass bulk behaviour is the focus and scale of the paper.

2.1 Flow Model

The combination of the conservation of mass of a single phase and Darcy's Law,

$$\frac{\partial(\phi\rho)}{\partial t} - \nabla \cdot \left(\frac{k}{\mu}\rho\left(\nabla P - \nabla\left(\rho g z\right)\right)\right) = q, \tag{1}$$

is used as the foundation of the flow model. Here ϕ is the porosity, ρ the fluid density, k the permeability, μ the fluid's dynamic viscosity, P the pore pressure, g the acceleration due to gravity, z the depth, and q the mass source terms. A fully implicit finite difference in time, finite volume in space framework (Aziz and Settari, 2002) is used to discretize the equation, which is then solved for the primary variable of pressure.

2.2 Mechanical Model

The mechanical model is based on the conservation of momentum,

$$\nabla \cdot \sigma^{'} + \nabla\left(\alpha P\right) = -f, \tag{2}$$

where $\sigma^{'}$ is the effective stress, α the Biot coefficient, and f represents the body forces. The sign convention is such that tension and extension are negative. This equation is then combined with the linear theory of poroelasticity (Biot, 1941; Rice and Cleary, 1976; Wang, 2000),

$$S_{ij} - \alpha P\delta_{ij} = \frac{E}{(1+\nu)}\epsilon_{ij} + \frac{E\nu}{(1+\nu)(1-2\nu)}\epsilon_{kk}\delta_{ij}, \tag{3}$$

in a finite element framework such that the stresses and strains associated with fluid production and injection can be solved for. Here, the total stress is represented by S, the Kronecker delta by δ_{ij}, the drained Young's Modulus by E, the drained Poisson's ratio by ν, and the strain by ϵ.

3 Problem Setup

The horizontal wells in this investigation will penetrate granitic basement rock, all at 4500 m depth, a similar depth to the EGS program of Soultz, France (Dorbath et al., 2009). The granitic basement rock is assumed to extend up to 2500 m depth, not unlike Basel EGS, Switzerland (Ladner and Häring, 2009). The overburden, however, will not be modelled and will be instead replaced with a constant applied stress based on a reasonable lithostatic pressure gradient. The model boundaries are chosen such that the wells are far enough away to limit their effect on the simulations. As shown in Figure 1, the entire set-up will be modelled in 2-D plane strain, an appropriate approach to model horizontal wells (Cheng, 2016). The investigation of the effects of preconditioning

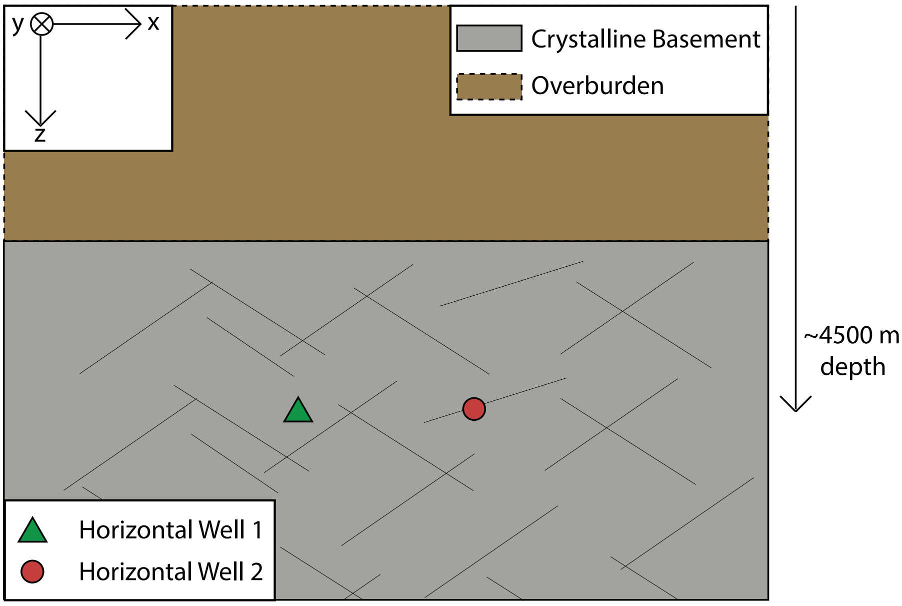

Fig. 1 Schematic of the problem setup for reverse and strike-slip faulting stress regimes. This represents a side view of two horizontal wells. The plane is normal to the orientation of the wells. The overburden is not modelled. Not to scale.

will be investigated for reverse, strike-slip, and normal faulting stress regimes. In each case, all three wells will be drilled parallel to S_{hmin}. Note that there are conflicting results regarding the orientation of reservoir creation during the stimulation of crystalline rock, with some operations indicating nearly parallel to S_{Hmax} (Häring et al., 2008; Kwiatek et al., 2019) and others indicating an offset such that reservoir creation occurs in the direction of strike of optimally oriented shear planes (Evans et al., 2005b; Kim et al., 2017, 2018) with it at times being difficult to determine exactly what happened in each case. It is further likely that the created reservoir geometry depends on the pre-existing discontinuities (Häring et al., 2008). For this reason and given observational inconsistencies, it is difficult to determine the optimum orientation of the wells with respect to the stress field.

The initial pore pressure and vertical stress are calculated using typical hydrostatic and lithostatic gradients, respectively. The assumption that the crust is critically stressed (Brudy et al., 1997; Townend and Zoback, 2000; Zoback and Townend, 2001; Zoback et al., 2002) is then used alongside the notion that the frictional strength of pre-existing faults is what limits the differential stress in the crust (Zoback and Healy, 1992; Brudy et al., 1997; Zoback and Harjes, 1997). This allows for the direct calculation of the minimum principal stress in the normal faulting stress regime and the maximum principal stress in the reverse faulting stress regime. For example, in a normal faulting stress regime, the minimum possible horizontal stress that could be present on a supposed optimally-oriented fault can be calculated using the vertical stress, the pore pressure, and the assumed coefficient of friction. This process is repeated at all depths to calculate the initial minimum principal stress everywhere in the model. In the strike-slip faulting stress regime, the maximum principal stress is calculated using this methodology after the minimum principal stress is assumed to be 0.8 times the vertical stress. The coefficient of friction will be assumed to 0.6, although there have been indications that the coefficient of friction in granitic rock may be higher (e.g., Blanpied et al. (1995)). It will be assumed that the frictional coefficient remains constant during stimulation, in agreement with laboratory studies (e.g., Ishibashi et al. (2018)).

A reasonable value of the intact Young's Modulus for granite is 36 GPa (Villeneuve et al., 2018). However, the rock is assumed to be fractured, meaning that, depending on the density of fractures, it may not be possible to use the intact Young's Modulus to describe the bulk behaviour (Villeneuve et al., 2018). Using a moderate fracture density and geological strength index, the rock mass Young's Modulus was taken as 50 % of the intact Young's Modulus based on findings by Villeneuve et al. (2018). This results in an equivalent Young's Modulus of 18 GPa. The Biot coefficient of this fractured granite is taken as 0.76, similar to that found by (Evans et al., 2003) for a fractured granite. The Poisson's ratio of the granite rock will be taken as 0.15, a relatively low value for granite due to its fractured nature (Walsh, 1965). A summary of the parameters used can be found in Table 1.

Table 1 *Model parameters*

Variable	Value	Unit
Fluid reference density (STP), ρ_f	1000	$\frac{kg}{m^3}$
Fluid compressibility, c_f	$5e-10$	$\frac{1}{Pa}$
Fluid dynamic viscosity, μ	0.001	$Pa \cdot sec$
Granite drained Young Modulus, E_g	$18e9$	Pa
Granite drained Poisson's Ratio, ν_g	0.15	$-$
Granite initial bulk porosity, ϕ_g	0.02	$-$
Granite Biot coefficient, $\alpha_{s,g}$	0.76	$-$
Coefficient of friction, μ_f	0.6	$-$

In order to avoid the compounding effects of thermal strains and to more clearly illustrate the effects of the stress preconditioning, the production and stimulation phases will be assumed to be isothermal (i.e., the reservoir will be assumed to be stimulated with water at reservoir temperature). This is obviously not a realistic scenario for a typical geothermal stimulation, and the probable effects of the thermal strains will be discussed in a later section.

3.1 Initial Bulk Permeability

Granite fractures can be assumed to have a high permeability (on the order of 10^{-12} m^2 (Ishibashi et al., 2018)) compared to granitic matrix, which generally has a permeability on the order of 10^{-21} to 10^{-20} m^2 (Morrow et al., 1986). For this reason, the matrix permeability will be assumed to be negligible compared to the fracture permeability, meaning that flow will be principally in the fractures, equivlanent to the level B distinction suggested by Cornet (2016), where flow is dominated by flow through reactivated fractures. In highly fractured and faulted crystalline rocks, the permeability of critically-stressed faults is much higher than that of faults which are poorly oriented for failure in the modern-day stress field (Barton et al., 1995). Evans et al. (2012) found in a study of European case histories, that all crystalline rock masses investigated were critically stressed. Therefore, the optimally-oriented faults and fractures in the granite investigated here will be assumed to be initially at least somewhat permeable, even if they need further shear stimulation to produce or inject fluid at rates sufficient for their given operational goal. This is supported by, for example, the pre-stimulation tests performed in granite in the Soultz HDR site and the Basel 1 enhanced geothermal system which yielded effective permeabilities of $3 \cdot 10^{-16}$ m^2 and 10^{-17} m^2 respectively (Evans et al., 2005b; Häring et al., 2008; Ladner and Häring, 2009). These tests also agree with the findings of Zoback and Townend (2001), who found that bulk permeability in the upper crust is high (10^{-17} m^2 to 10^{-16} m^2) due to critically-stressed faults. For this reason a starting value of 10^{-17} m^2 is used for bulk permeability, a value on the low end of bulk permeabilities seen in the field as mentioned above. The actual initial value of the permeability seen in the simulation will be lower than this value due its dependence on pressure and stress addressed in Section 3.2.

3.2 Shear Stimulation

Although stimulation in Enhanced Geothermal Systems may well be mixed mode between the creation of new fractures and the shearing of old fractures and faults (McClure and Horne, 2014; Norbeck et al., 2018) (especially with injection pressures above the minimum principal stress), it is thought that shear failure is the dominant and most promising mechanism of reservoir creation in hard rock formations in EGS stimulation (Evans et al., 2005b; Ziagos et al., 2013; Zang et al., 2014). Indeed, it has been previously shown in laboratory (e.g., Chen et al. (2000); Ishibashi et al. (2018)) and field (e.g., Jupe et al. (1992); Evans et al. (2005b); Ladner and Häring (2009); Guglielmi et al. (2015)) studies of granitic rock that fracture permeability increases with shear displacement. In this study specifically, it will be assumed that the fractures and faults optimally oriented for shear in the prevailing stress field will be the planes upon which shear failure occurs, as seen, for example at Soultz (Evans et al., 2005b).

Shear stimulation of granitic reservoirs results in a permeability increase that can vary depending on the site, even varying within the same well (Evans et al., 2005a). For example, permeability was increased by three orders of magnitude at the Fjällbacka Hot Dry Rocks Project, Sweden following stimulation

(Jupe et al., 1992), but Soultz, France only saw an increase in transmissivity of a factor of fifteen when the effect of the stimulation is evaluated over the entire wellbore (Evans et al., 2005a). Here, stimulation will be assumed to ultimately result in a permeability increase of a factor of 200, similar to the results of stimulation at Basel (Ladner and Häring, 2009) and the 1993 stimulation of a 550 m section of hole at Soultz (Evans et al., 2005a).

The permeability used in the numerical model will be based on the notion of a changing aperture width with effective normal stress and a stepwise change in permeability occurring after a failure condition is reached (Miller and Nur, 2000; Miller, 2015). As in Miller (2015), permeability is assumed to take the form

$$k = k_0 e^{\frac{-\bar{\sigma_n}}{\sigma^*}}, \tag{4}$$

where k_0 is the initial permeability defined in Section 3.1, $\bar{\sigma_n}$ is the effective normal stress acting on the assumed shear plane, and σ^* is a normalizing constant taken as 100 MPa. The normalizing constant is picked as a large value such that the initial individual values of permeability in the reservoir are not significantly lower than the overall values of bulk permeability seen in the EGS reservoirs in Section 3.1. Again following the model used by Miller (2015), the failure planes (with one assumed orientation for each reservoir block) will follow an unbounded normal distribution with a mean orientation corresponding to the optimal orientation in the given stress regime and a standard deviation of 0.02 radians. As the standard deviation is small, this is, in essence, equivalent to using a von Mises distribution with a large concentration coefficient. Note that this model implies, based on the assumed critically-stressed nature of the reservoir, that minuscule changes in stress or pore pressure could result in shear failure if a given cell is optimally oriented. In fact, however, it will be assumed that all cells require a Coulomb stress increase of 0.1 MPa before failure in addition to any stress increase required due to a non-optimal orientation. A 0.1 MPa Coulomb stress increase is a reasonable valuable for the initiation of slip (Stein, 1999). Coulomb stress, τ, is defined as

$$\tau = \tau_s - \mu_f \left(S_n - P\right), \tag{5}$$

where τ_s and S_n are the shear stress and normal stress on a potential shear plane (for calculations of Coulomb stress this plane is assumed to be optimally oriented in the prevailing stress regime) and μ_f is the static coefficient of friction. Generally, the Coulomb stress will increase when the maximum principal total stress increases, the minimum principal total stress decreases, or the pore pressure increases.

If the Coulomb failure criteria for a given cell is reached, a stepwise change in permeability will occur (Miller and Nur, 2000; Miller, 2015) such that k_0 in Equation 4 will be replaced by k_0'; where k_0' is defined as

$$k_0' = x k_0. \tag{6}$$

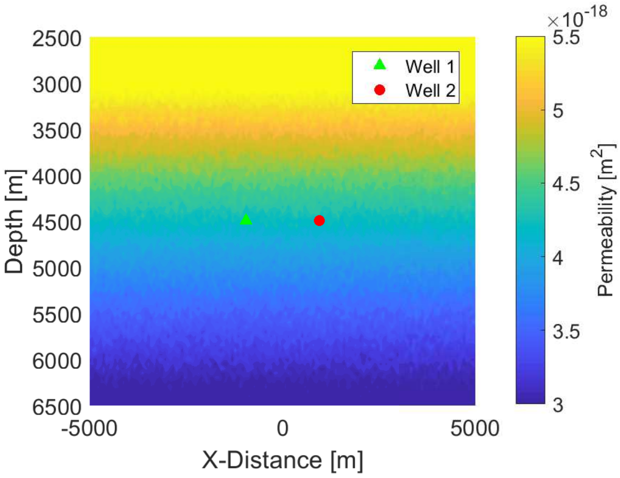

Fig. 2 The initial permeability field used in the reverse faulting case. The heterogeneity is due to the randomness associated with the permeability model.

Here, x is a multiplication factor taken to be equal to 200 based on the reviewed stimulation treatments mentioned above. This methodology for modelling permeability enhancement due to shear stimulation implies that permeability enhancement largely remains after high pressure is stopped. This is representative, for example, of the shear stimulation at the Soultz HDR site (Evans et al., 2005b). Note that porosity is kept constant throughout the simulation, reflecting, for example, the methodologies of Miller and Nur (2000) and Baisch et al. (2010). This means that the coupling between the mechanical model and the flow model is entirely contained in the change of permeability. An example of the permeability field, Figure 2, is shown for the reverse faulting case. Although the permeability fields of each run will vary slightly due to the randomness associated with the permeability model, this variation is limited and the general trends predicted by the results are repeatable.

4 Results

This section will be subdivided into three subsections, one subsection for each stress regime, Table 2. Beginning with a reverse faulting stress regime, two wells will be stimulated with the goal of connecting the stimulated regions of each well to create a doublet system. In the reverse faulting case, the comparison will be made between the case where the first well is flowback after its stimulation and the case where this first well is not flowback after stimulation and instead the second well is stimulated immediately. For the remaining stress regimes, however, the flowback case will not be presented and instead the effect of the first stimulation treatment on the second will be shown by comparing the average propagation lengths of the stimulated region outside of the two wells and inside the two wells.

Table 2 *Principal stress orientations.* The wells are drilled in the y-direction; however, the orientations of the principal stresses change depending on the stress regime. Note that S_x is S_{Hmax} and S_y is S_{hmin} in each case.

Regime	S_1	S_2	S_3
Reverse Faulting	S_x	S_y	S_z
Strike-Slip Faulting	S_x	S_z	S_y
Normal Faulting	S_z	S_x	S_y

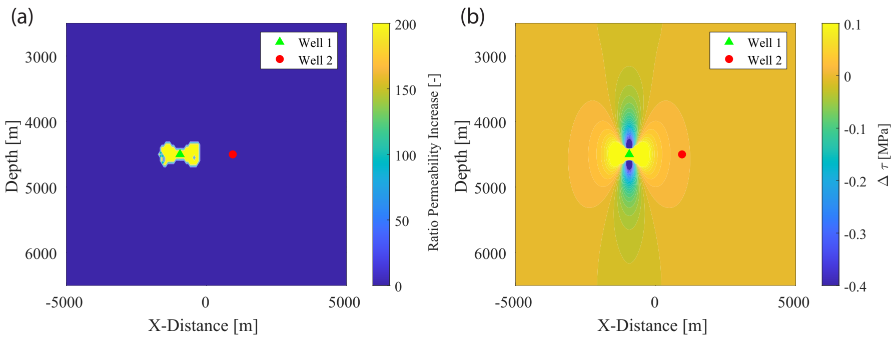

Fig. 3 The result of the stimulation of well 1 in the reverse faulting stress regime case. (a) The permeability enhancement associated with the stimulation treatment (t=3 days). (b) The Coulomb stress changes resulting from the stimulation treatment (t=3 days).

4.1 Reverse Faulting

In a reverse faulting stress regime, the maximum principal stress is horizontal and the minimum principal stress is vertical. Therefore, increases in the total horizontal stress (specifically the maximum horizontal stress, S_{Hmax}) and decreases in the total vertical stress will generally result in an increase in Coulomb stress.

In this case, the two wells will be located at a depth of 4500m and separated by 1884m, with the midpoint between the two wells having an X-Distance coordinate of 0m, Figure 2. The stimulation treatment procedure is begun by first stimulating the left-most of the two wells with an injection rate of 0.014 $\frac{kg}{msec}$, which corresponds to 7.0 $\frac{kg}{sec}$ for a 500 m long well length section, over a period of three days. This stimulation treatment would be similar to, but slightly smaller than, the 2000 stimulation of GPK2 at Soultz-sous-Forêts, for example (Dorbath et al., 2009). The permeability increases and Coulomb stress changes associated with this stimulation treatment are shown in Figure 3.

Next, the first well is flown back with a rate of 2.33 $\frac{kg}{sec}$ over a period of 9 days, resulting in the entire fluid mass that was injected with the stimulation treatment being reproduced. Note that it is probably unlikely that the entire injected mass would be reproduced in reality; however, the purpose here is simply to illustrate the effect of flowback on the far-field poroelastic stresses. The permeability above and below the previously stimulated region increases slightly during this flow back period, Figure 4a. This is due to production in-

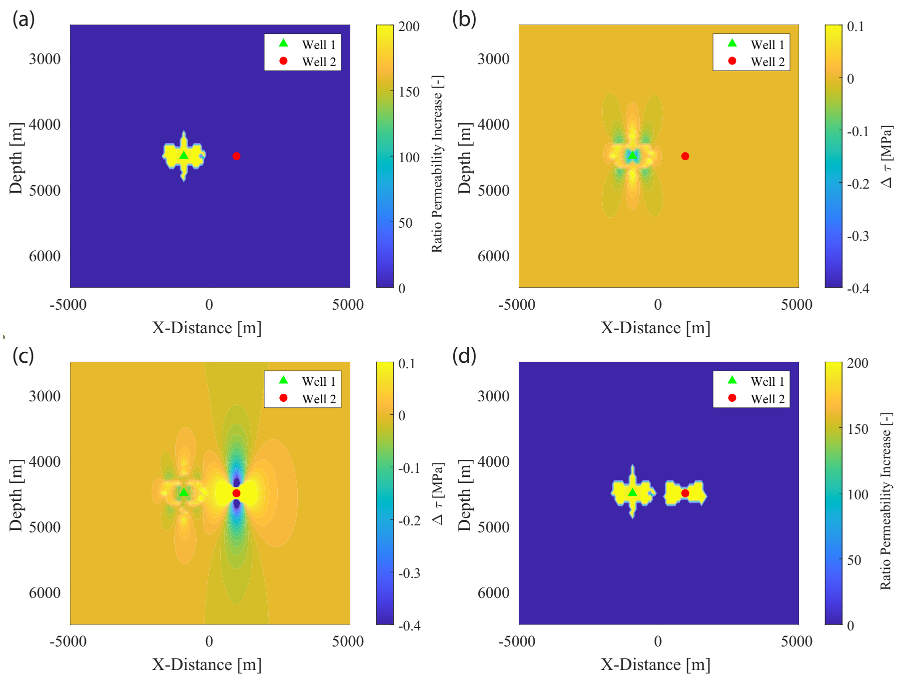

Fig. 4 For the reverse faulting stress regime case, the result of flowing back the first well before stimulating the second well. (a) The permeability enhancement at a time immediately after the flowback period (t=12 days), note the enhancement that has occurred above the initially stimulated region. (b) The Coulomb stress at a time immediately after the flowback period of the first well (t=12 days). The Coulomb stresses in-between the two wells has been reduced since the initial stimulation treatment, when compared to Figure 3b. (c) The Coulomb stresses after the stimulation of the second well (t=15 days). (d) The permeability enhancement at the end of the entire procedure (t=15 days). The two wells are not connected with a separation of the two stimulated zones of 362m.

ducing increased total horizontal stresses and decreased total vertical stresses in this region. The Coulomb stress changes associated with this flowback period, Figure 4b, show the result of these stress changes with increases above and below the previously stimulated region. This type of increased Coulomb stress and shear failure occurring above production zones is analogous to the reverse faulting sometimes seen during hydrocarbon production (e.g., Segall (1989)). Figure 4b also indicates that the Coulomb stress in-between the two wells has decreased since flowback began, when compared to Figure 3b. The changes to pore pressure and the maximum and minimum principal stresses are shown in Figure 5.

At this stage, the second well is stimulated using the same stimulation treatment that was used in the first well. The Coulomb stress changes, Figure 4c, and permeability field enhancements, Figure 4d, indicate that the two stimulated zones were not connected in this case, being still separated by 362m of unstimulated rock mass.

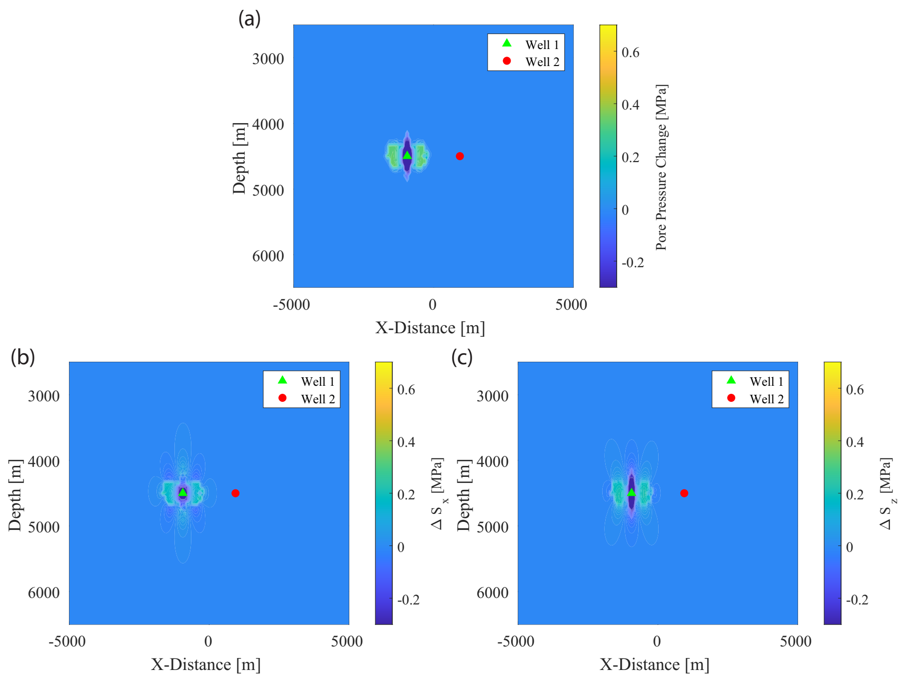

Fig. 5 For a reverse faulting stress regime, the (a) pore pressure changes, (b) maximum principal total stress changes (ΔS_x for reverse faulting), and (c) minimum principal total stress changes (ΔS_z for reverse faulting) after stimulation and flowback of the first well.

If, instead of flowing back the well, the well is simply shut-in and the second stimulation begun immediately after the termination of the first, the Coulomb stress changes associated with the first stimulation will largely remain during the second stimulation. As these Coulomb stress changes are encouraging failure and are larger closer to the first well, they may potentially cause the stimulation treatment of the second well to be directed towards the stimulated zone of the first well.

To test this procedure, the first well is stimulated as before with an injection rate of 7.0 $\frac{kg}{sec}$ over three days. Following this, the second well is stimulated immediately after the first stimulation treatment with no flowback period. The stimulation treatment again consists of an injection rate of 7.0 $\frac{kg}{sec}$ over three days. In this way, the Coulomb stress changes associated with the first stimulation treatment remain and help to ensure connection between the two wells' stimulated regions.

At the midpoint between the two wells, the Coulomb stress just before the second stimulation had increased by 0.056 MPa, Figure 3b. However, at the location of equivalent distance from well 2 but in the opposite direction (a depth of 4500m and an X-distance of 1884m), the Coulomb stress just before the second stimulation has only increased by 0.0056 MPa. These differences in Coulomb stress change are what ultimately cause the stimulation of well 2 to

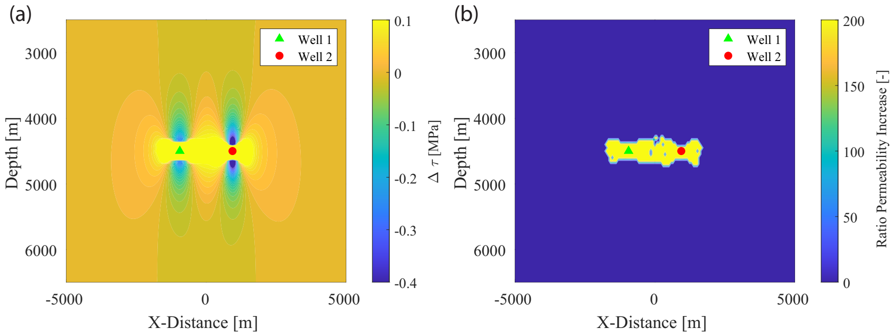

Fig. 6 For the reverse faulting stress regime case, the result of not flowing back the first well before beginning the stimulation treatment of the second well. (a) The Coulomb stresses after the stimulation of the second well (t=6 days). (b) The permeability enhancement at the end of the entire procedure (t=6 days). The stimulated zone of each well extends and average 761m away from the other doublet well and 942m towards it.

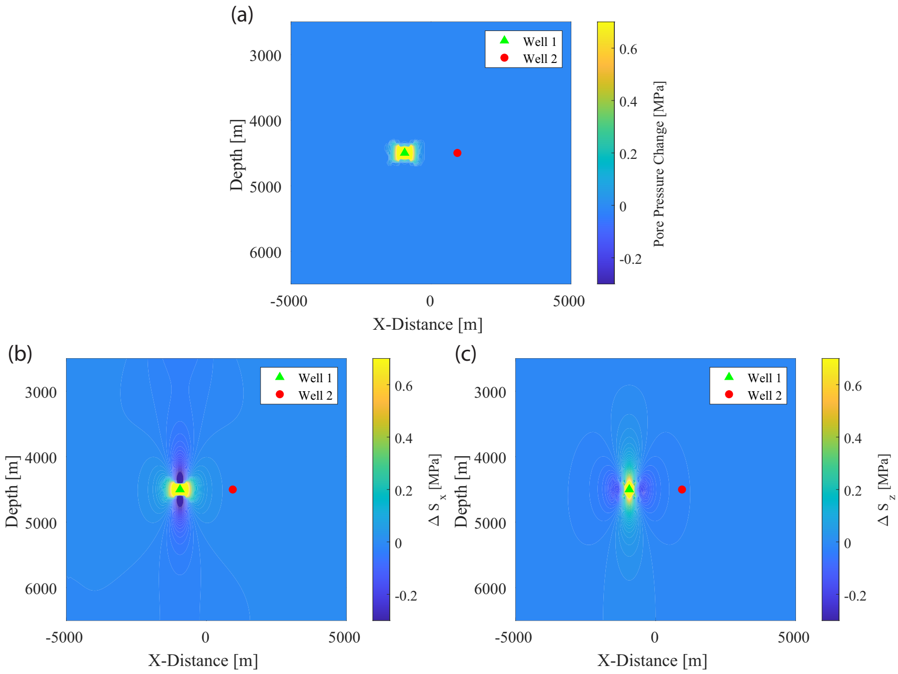

Fig. 7 For a reverse faulting stress regime, the (a) pore pressure changes, (b) maximum principal total stress changes (ΔS_x for reverse faulting), and (c) minimum principal total stress changes (ΔS_z for reverse faulting) associated with the stimulation of the first well without flowback. Note how, in the region between the two wells, the maximum principal total stress increases, the minimum principal total stress decreases, and the pore pressure remains unchanged. These changes explain the Coulomb stress changes seen in Figure 3b and indicate that the stress is being preconditioned due to total stress changes, not pore pressure changes. It is useful to compare this figure to Figure 5.

be directed towards the stimulated region of well 1 as opposed to propagating equal distances in both directions. In fact, the stimulation treatments of both wells, on average, propagate 761 m away from the other doublet well and 942 m towards it, Figure 6b, meaning that the stimulated zones extend over 20% farther in-between the two wells than they do on the outside of the two wells. Note that the average stimulation length of each well here is similar to, for example, the seismicity cloud resulting from stimulation at Soutlz-sous-Forêts, which extended over 1000 meters horizontally and 500 meters vertically (Evans et al., 2005b).

Unlike the results shown by Baria et al. (2004), the direction of the stimulation treatment here is accomplished entirely by changes in stress, not pore pressure. At an X-Distance of 0 (the center point between the two wells - 942m from each well), the pore pressure change after the stimulation of the first well is zero. The change in the S_{Hmax}, however, is 0.045 MPa, and results in over half of the Coulomb stress change required for failure, Figure 7.

For the remaining two stress regimes, a flowback case will not be shown. Instead, the average distances of propagation will be used to demonstrate the degree to which the stimulation treatment was effectively directed.

4.2 Strike-Slip Faulting

In a strike-slip faulting stress regime, the maximum and minimum principal stresses are both horizontal. The stress changes induced by injection through a horizontal well will be anisotropic. For example, during the stimulation of the first well, Figure 8a and b, the horizontal stress perpendicular to the first well will experience greater compressive changes than the horizontal stress parallel to it at large distances. Assuming the well is drilled parallel to the minimum principal stress, this means that the maximum principal stress will increase (becoming more compressive) more than the minimum principal stress, resulting in an increase in differential stress and Coulomb stress. These Coulomb stress changes will be more pronounced near the stimulated region of the first well, meaning that the stimulation treatment of the second well will be more likely to propagate towards the first well than in the other direction. In this case, the two wells will be located at a depth of 4500m and separated by 1450m, with the midpoint between the two wells having and X-Distance coordinate of 0m.

The stimulation treatment procedure is begun by first stimulating the leftmost of the two wells with a stimulation rate of 0.0247 $\frac{kg}{msec}$, which corresponds to 12.37 $\frac{kg}{sec}$ for a 500 m long well length section, over a period of three days, Figure 8a. This stimulation treatment would be similar to, but slightly smaller than, the 2000 stimulation of GPK2 at Soultz-sous-Forêts, for example (Dorbath et al., 2009). Next, injection into the first well is stopped and the second well is stimulated with exactly the same stimulation treatment. The first well does not undergo a flowback period before the stimulation of the second well.

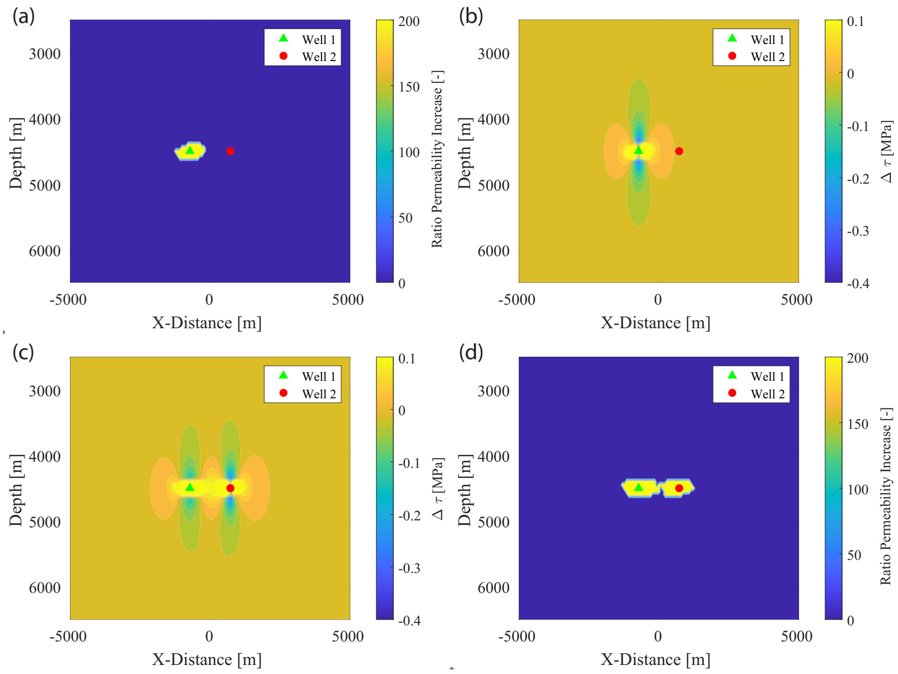

Fig. 8 The result of the stimulation treatment in a strike-slip faulting stress regime. (a) The permeability enhancement associated with the stimulation treatment of the first well (t=3 days). (b) The Coulomb stress changes resulting from the stimulation treatment of the first well (t=3 days). (c) The Coulomb stresses after the stimulation of the second well (t=6 days). (d) The permeability enhancement at the end of the entire procedure (t=6 days). The stimulated zone of each well extends and average 543m away from the other doublet and 725m towards it.

At the midpoint between the two wells, the Coulomb stress just before the second stimulation has increased by 0.042 MPa, Figure 8b. However, at the location of equivalent distance from well 2 but in the opposite direction (a depth of 4500m and an X-distance of 1450m), the Coulomb stress just before the second stimulation has only increased by 0.004 MPa. These differences in Coulomb stress change are what ultimately cause the stimulation of well 2 to be directed towards the stimulated region of well 1 as opposed to propagating equal distances in both directions. In fact, the stimulation treatments of both wells, on average, propagate 543 m away from the other doublet well and 725 m towards it, Figure 8d, meaning that the stimulated zones extend over 30% farther in-between the two wells than they do on the outside of the two wells.

This change in Coulomb stress that guides the stimulation treatment of the second well towards the first well is caused by changes in total stress, not changes in pore pressure. At the midpoint of the two wells, the change in the maximum horizontal stress just before the second stimulation is 0.145 MPa whereas the change in the pore pressure is 4e-7 MPa, Figure 9.

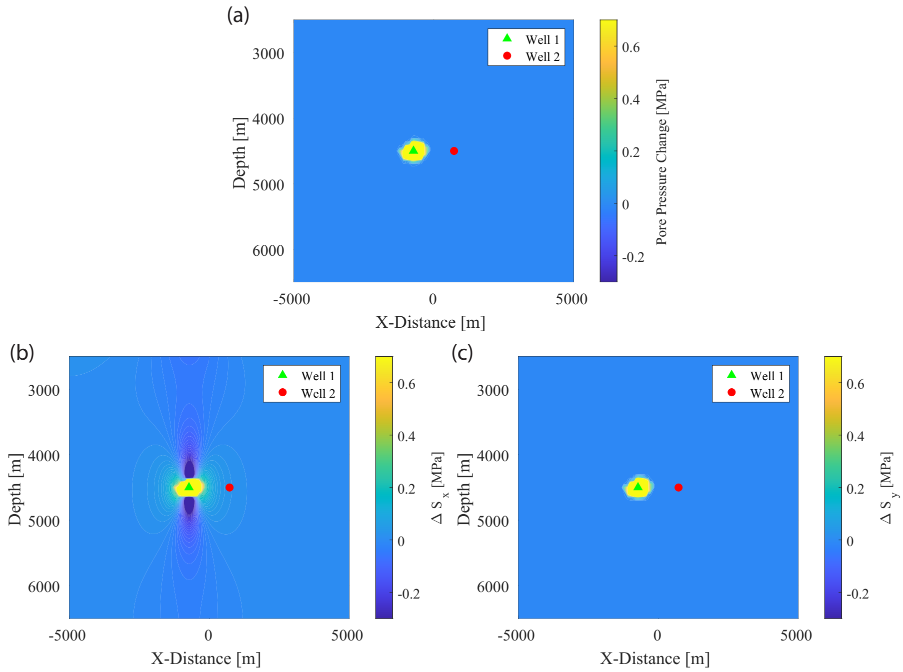

Fig. 9 For a strike-slip faulting stress regime, the (a) pore pressure changes, (b) maximum principal total stress changes (ΔS_x for strike-slip faulting), and (c) minimum principal total stress changes (ΔS_y for strike-slip faulting) associated with the stimulation of the first well without flowback. Note how, in the region between the two wells, the maximum principal total stress increases, whereas the minimum principal total stress and pore pressure remain unchanged. These changes explain the Coulomb stress changes seen in Figure 8b and indicate that the stress is being preconditioned due to total stress changes, not pore pressure changes.

4.3 Normal Faulting

In a normal faulting scenario, the vertical stress is the maximum principal stress. In the case that two doublet wells are drilled horizontally in a direction parallel to the minimum principal stress, the injection-induced poroelastic stress changes caused by the stimulation of the first well will be expected to increase the total vertical stress primarily in locations above and below the stimulated well. This implies that the poroelastic stress changes will primarily encourage shear failure in locations which are vertically in-line with the well and not those horizontally in-line. For this reason, the wells are aligned vertically with a separation of 1000m at depths of 3500m and 4500m.

The stimulation treatment procedure is begun by first stimulating the shallower of the two wells with a stimulation rate of 0.0125 $\frac{kg}{msec}$, which corresponds to 6.25 $\frac{kg}{sec}$ for a 500 m long well length section, over a period of three days, Figure 10a. This stimulation treatment would be similar to, but slightly smaller than, the 2000 stimulation of GPK2 at Soultz-sous-Forêts, for example (Dorbath et al., 2009). Next, injection into the first well is stopped and the second well is stimulated with exactly the same stimulation treatment. The first well does not undergo any flowback period before the stimulation of the second well.

At the midpoint between the two wells (a depth of 4000m and an X-distance of 0m), the Coulomb stress just before the second stimulation has increased by 0.047 MPa, Figure 10b. However, at the location of equivalent distance from well 2 but in the opposite direction (a depth of 5000m and an X-distance of 0m), the Coulomb stress just before the second stimulation has only increased by 0.002 MPa. These differences in Coulomb stress change are what ultimately cause the stimulation of well 2 to be directed towards the stimulated region of well 1 as opposed to propagating equal distances in both directions. In fact, the stimulation treatments of both wells, on average, propagate 400 m away from the other doublet well and 500 m towards it, Figure 10d, meaning that the stimulated zones extend 25% farther in-between the two wells than they do on the outside of the two wells.

This change in Coulomb stress that guides the stimulation treatment of the second well towards the first well is caused by changes in total stress, not changes in pore pressure. At the midpoint of the two wells, the change in the vertical stress just before the second stimulation is 0.159 MPa whereas the change in the pore pressure is 1.65e-5 MPa, Figure 11.

5 Discussion

5.1 Assumptions

5.1.1 Isothermal Simulations

The influence of temperature has not been considered in the analyses although temperature-induced stresses may play a significant role during EGS stimulation (e.g., Ghassemi and Tao (2016)). This was primarily done to simplify the analyses and more clearly illustrate the effects of stress preconditioning. In case-specific applications of this methodology, temperature effects should be considered. In fact, it may even be possible to design a stimulation procedure such that temperature-change induced stresses further precondition the stress field in a beneficial manner.

To evaluate the influence of the temperature-change induced stresses such that their neglection can be justified, the flow model was extended to include the conservation of energy,

$$\frac{\partial H_m}{\partial t} + \nabla \cdot \Gamma + \nabla \cdot f_t = q_T, \tag{7}$$

where H_m is the enthalpy of the entire medium, Γ is the heat conduction, f_T is the convection, and q_T represents the source terms. The equation is discretized and solved fully implicitly with the mass conservation equation, yielding both pressure and temperature. Equilibrium is assumed between the fluid and rock

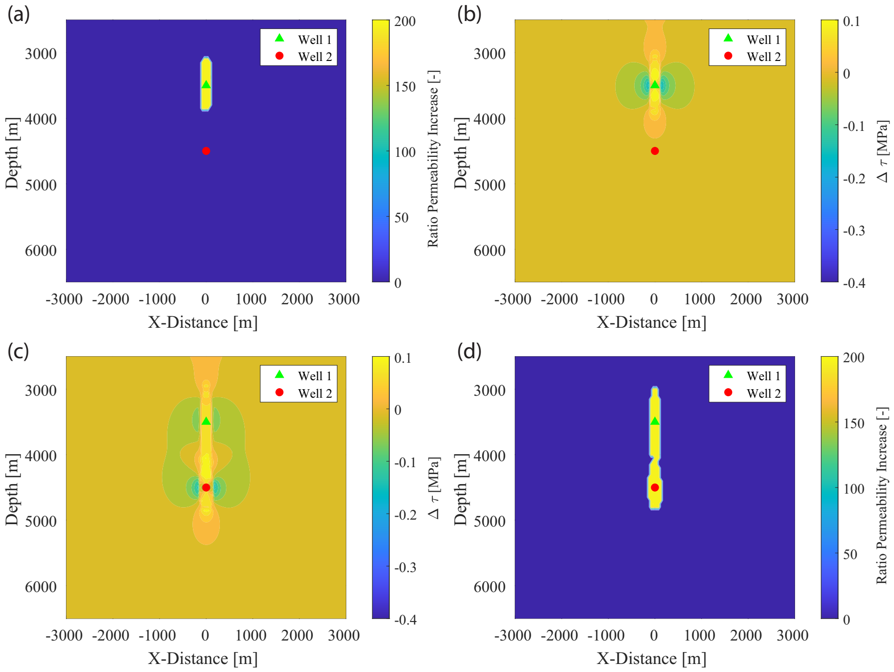

Fig. 10 The result of the stimulation treatment in a normal faulting stress regime. (a) The permeability enhancement associated with the stimulation treatment of the first well (t=3 days). (b) The Coulomb stress changes resulting from the stimulation treatment of the first well (t=3 days). (c) The Coulomb stresses after the stimulation of the second well (t=6 days). (d) The permeability enhancement at the end of the entire procedure (t=6 days). The stimulated zone of each well extends and average 400m away from the other doublet and 500m towards it.

temperature in each cell. To simplify the analysis, the fluid density and viscosity are assumed to remain constant with change in temperature. In the mechanical model, the thermal strain, ϵ_T,

$$\epsilon_T = \alpha_T \Delta T, \tag{8}$$

is added to the mechanical strains before the computation of stress changes. Here, α_T is the coefficient of linear thermal expansion and T is the temperature. A surface temperature of 30 ^0C and a thermal gradient of 0.035 $\frac{^0C}{m}$ are assumed. The thermal conductivity of the water and granite are assumed to be 0.67 and 2.5 $\frac{W}{mK}$ respectively. The heat capacity of the water and granite are assumed to be 4183 and 950 $\frac{J}{kgK}$ respectively. The coefficient of linear expansion of granite is taken as $40 \cdot 10^{-6}$ $\frac{1}{^0C}$, and the fluid enters the reservoir at a temperature of 47 ^0C.

Using this updated model, the reverse faulting case was rerun up to the point just before the second stimulation. At the midpoint between the two wells, the difference in change in Coulomb stress in this case and in the case presented previously where temperature effects were not considered is 0.0002

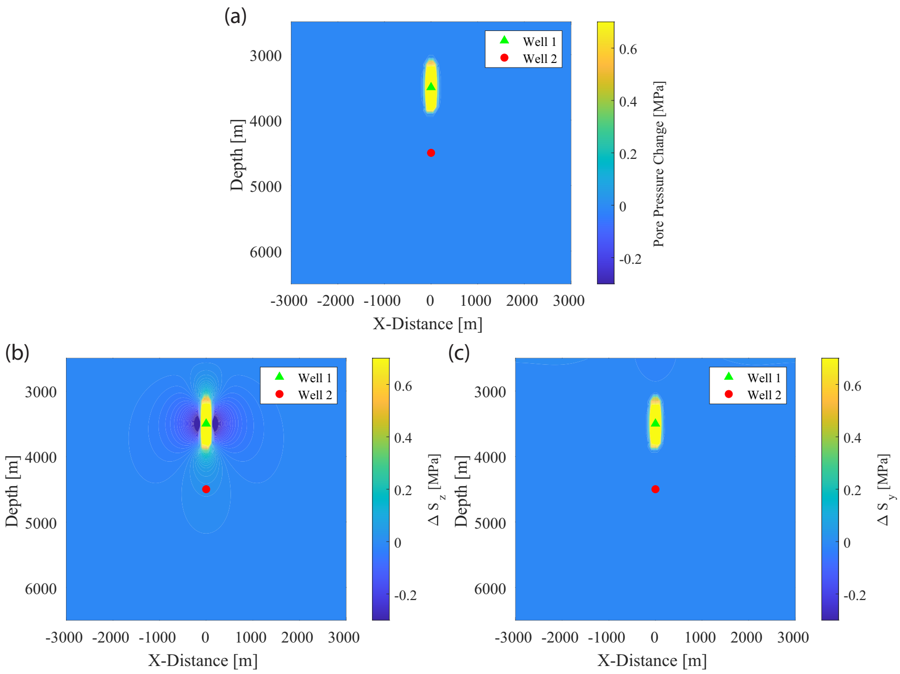

Fig. 11 For a normal faulting stress regime, the (a) pore pressure changes, (b) maximum principal total stress changes (ΔS_z for normal faulting), and (c) minimum principal total stress changes (ΔS_y for normal faulting) associated with the stimulation of the first well without flowback. Note how, in the region between the two wells, the maximum principal total stress increases, whereas the minimum principal total stress and pore pressure remain unchanged. These changes explain the Coulomb stress changes seen in Figure 10b and indicate that the stress is being preconditioned due to total stress changes, not pore pressure changes.

MPa. Considering that the Coulomb stress change due only to poroelastic effects was 0.056 MPa, this justifies not including stress changes due to temperature in the model. These Coulomb stress changes are small due to the small temperature changes of the system. The small temperature changes are due to the relatively small injection volumes (approximately 1620 m^3 over 500 m of wellbore over 3 days). In order to keep the model as simple as possible and better illustrate the effects of poroelastic stress changes, the effect of temperature is therefore not included in the model.

5.1.2 Stress Criticality

In the simulations presented here, the reservoir was assumed to be critically stressed based on findings by Evans et al. (2012). In reality, however, knowledge of the in situ stress state is very important for reservoir stimulation activities, and the state of stress should ideally be investigated in each case before the start of operations. If the crust is less critically stressed than in the presented cases, larger pore pressure changes will be needed to stimulate the reservoir as shear failure would become more pore-pressure dominated. The poroelastic stresses that guide the second stimulation treatment will make up less of the required changes for failure. For instance, in this case it was assumed that a Coulomb stress change of 0.1 MPa is required to induce shear failure. The Coulomb stress change induced by the preconditioning at the mid-point between the wells was approximately 0.05 MPa, meaning that it made up half of the required stress change. However, if the required Coulomb stress change was instead 0.5 MPa, this preconditioning stress would only make up ten percent of this value and it would presumably play a smaller role in directing the second stimulation treatment. Conversely, this would mean larger pore pressure changes would have been needed to stimulate the first well. This would result in larger induced poroelastic stress changes.

5.1.3 Stress Redistribution

The model used here does not include stress redistribution associated with shear failure occurring during stimulation. Previous studies (e.g., Catalli et al. (2013)) have shown that stress redistribution associated with shear failure during hydraulic stimulation can have a significant impact on future events. Indeed, stimulation treatments of granitic rock have been shown to be capable of altering the stress field through aseismic slip occurring within the stimulated zone (e.g., Cornet and Julien (1989); Schoenball et al. (2014)). Although these stress changes have been shown to be large (on the order of ten MegaPascals), they are thought to be largely confined to the stimulated region (Schoenball et al., 2014). It is possible to come up with a far-field estimate of this effect, if, for example, the Coulomb stress changes occurring near the location of the second well can be calculated assuming the energy release equivalent to a dynamic earthquake of M_w 3.0 occurring at the wellbore of the first well. This amount of energy release due to aseismic slip is approximately equal to that which occurred at the Le Mayet de Montagne granitic test site (Cornet, 2016). An M_w 3.0 earthquake corresponds to a fault length of approximately 330 m according to typical earthquake scaling laws (Stein and Wysession, 2003). King et al. (1994) found unclear correlations between aftershocks and Coulomb stress changes after distances of about 3 fault lengths, which is less than the separation between the two wells in each of the three cases presented. Given that correlation between stress changes and aftershocks was seen for positive Coulomb stress changes of the order of 0.01 MPa (King et al., 1994), the stress changes associated with aseismic slip in the reservoir at the location of the second well are most likely not significantly larger than the poroelastic stress changes induced by the treatment itself (0.05 MPa at the midpoint of the two doublet wells in the reverse faulting case where the well separation is the largest). Therefore, although it would be unreasonable to claim that stress changes associated with slip in the stimulated zone of the first well are negligible for the stimulation of the second well, it can be concluded that the poroelastic stress changes are significant in their own right.

For this reason, the poroelastic stress changes shown here may still be significant enough to direct a given stimulation treatment. However, in order to better evaluate the possibility of directing a stimulation treatment, the effect of the stress redistribution associated with the events occurring during the first stimulation treatment on the far-field stresses should be investigated, for example with a Mohr-Coulomb plasticity model. Regardless of whether this stress preconditioning methodology is employed or not, stress redistribution associated with shear failure in the stimulated region of the first well is likely to occur.

5.1.4 Use of an Equivalent Continuum Plane Strain Elastic Model

These investigations could have been performed with a discontinuum model instead of the equivalent continuum approach implemented here. Discontinuum models, where fractures are explicitly modelled, represent a large body of literature with many recent technical developments and applications to EGS modelling (e.g., McClure and Horne (2014); Ţene et al. (2017)). These models are better equipped than equivalent continuum models to predict small-scale behaviour and are generally able to more realistically replicate a specific site's response to fluid injection. However, these models are generally more computationally expensive and require longer simulation times than equivalent continuum models. Indeed, equivalent continuum models are capable of investigating the effects of fluid injection in a fractured media, and can be especially useful for larger-scale simulations, such as those performed here. These use of equivalent continuum models for fractured-media simulations has been addressed previously (Oda, 1986; Miller, 2015; Gan and Elsworth, 2016).

The use of a 2-D plane strain model over a 3-D or generalized plane strain model (e.g., Cheng (1998)) is valid when the wellbore is long compared to its diameter and in-line with one of the principal stress directions (Cheng, 2016). It is possible, however, that out-of-plane displacements, especially near the heel and toe of the wells, might alter the results slightly. In these regions, during the fluid injection, it is likely that changes to the principal total stress parallel to the wellbore will be slightly reduced if this effect is included.

The mechanical model used here is also entirely elastic. It is probable that a more rigorous approach would alter the magnitude of the stress changes found. For example, Pijnenburg et al. (2018) recently showed that the use of an elastic simulator during the modelling of fluid production in a sandstone likely under-predicts strains and over-predicts total stress changes in the case that the deformation is inelastic. Essentially, the use of a linear elastic simulator here corresponds to the assumption that the non-linear responses of the system remain localized such that the mechanical behaviour of the rock mass as a whole can be well represented by such a linear elastic model (Cornet, 2016).

Further, certain parameters are likely to change throughout the stimulation procedure. For example, the relatively low Poisson's ratio chosen due to the fractured nature of the rock is likely to increase as shear failure occurs (Walsh, 1965). This would have implications for the magnitude of the changes to each component of the stress tensor. Deformation-induced porosity changes were also not accounted for here; an effect which may quantitatively influence the results. It is also probable in reality that many of the poroelastic parameters used here vary with effective stress (e.g., Walsh (1965); Bernabé (1986)). This variation was not accounted for in the analyses performed here, unlike in other equivalent continuum models applied to EGS (e.g., Gan and Elsworth (2016)).

5.2 Implications

Variations on this approach could be imagined. For example, stimulating both wells at the same time would allow for both wells to benefit from advantageous stress changes. However, each well would experience less preconditioning Coulomb stress changes than the second well experienced during these simulations. This is due to the fact that the pore pressures will not yet have reached their post-stimulation values. Additionally, this approach would require sufficient pumping power to stimulate two wells at once. Another possibility would be to use the poroelastic and thermoelastic stress changes associated with an existing doublet-well system to direct the stimulation treatment of a third well. This would presumably incur larger stress changes than those used here and would allow for the more efficient direction of the stimulation of the third well.

It should be noted that one possible drawback to not flowing back the wells is the possibility of inducing a large seismic event. Frequently these large magnitude events occur after stimulation activities have been stopped (e.g., (Häring et al., 2008; Kim et al., 2018)), and it has even been suggested that flowing the wells back could help prevent seismicity (McClure, 2015). Despite this, the methodology proposed here is designed to use the built up poroelastic stresses due to the increased pore pressure associated with injection to facilitate the stimulation of another well. As shown in Section 4.1, flowing the well back makes this process significantly less effective.

The successful implementation of this methodology would yield a number of advantages. Engineers would have higher confidence in connecting two wells separated by a given distance when using this methodology as opposed to the case where the wells are flown back before the next stimulation. Alternatively, wells could be separated by a larger distance, reducing the risk of short-circuiting and increasing the contact time of the circulating fluid with the reservoir. Additionally, because this methodology encourages the second stimulation treatment to advance towards the first well, it seems less likely that this stimulation treatment will stimulate a large fault as the total stimulated reservoir volume is reduced for a given well separation distance. Further, it can be imagined that this type of technique could be implemented in combination with other similar techniques, such as fluid production, to provide reservoir engineering solutions for large-scale reservoir creation. Of course, the ability to influence the direction of a stimulation treatment does not mean that operators have total control over how the stimulation treatment propagates, simply that the stimulation treatment is guided such that it is more likely to advance in a certain direction.

5.3 Future Outlook

These results potentially have implications for hydraulic fracturing. Although not directly applicable, it has been shown that poroelastic stress changes during injection are able to alter the stress field and affect a shear stimulation. Mode I fracturing depends on the pore pressure overcoming the minimum principal stress. It can therefore be imagined that both injection and production are capable of altering the minimum stress such that mode I fracture propagation is either attracted to or repelled from a particular region of a reservoir. In fact, it has already been shown that hydraulic fracture propagation is affected by pre-existing injection and production wells (e.g., Berchenko and Detournay (1997); Gao et al. (2019)). Further investigations should be performed on how to purposefully use these stress changes to help direct hydraulic fracturing treatments.

The numerical results found here indicate that a shear stimulation treatment can be directed in a critically-stressed crust. Following this, experimental work should be carried out to try to achieve these results in a real experimental rock laboratory. Should those experiments be successful, other methodologies for directing stimulation treatments should be investigated, especially ones capable of directing stimulation treatments in less critically-stressed reservoirs.

6 Conclusion

In this work, shear stimulation treatments in critically-stressed fractured granitic rock from horizontal wells have been directed via the stress changes associated with a previous stimulation to preconditioning the stress field for the next stimulation. These stress changes increase the Coulomb stress primarily in the region between the two wells which results in the stimulation treatment of the second well preferentially propagating towards the first. These results have implications for reservoir engineering applications in EGS reservoirs. Further research should be performed to both confirm the results in meso-scale field demonstrations and develop methodologies for directing stimulation treatments in less critically-stressed reservoirs.

Acknowledgements This work has been supported by a research grant (SI/500963-01) of the Swiss Federal Office of Energy and a student grant from the Swiss Association of Energy Geoscientists. Xiaodong Ma received funding from the Swiss Competence Center for Energy Research - Supply of Electricity and Swiss National Science Foundation Grant No. 182150. The authors would like to thank two anonymous reviewers for their comments and insights, which greatly improved the quality of the manuscript. No new data were used in producing this manuscript.

References

Aziz K, Settari A (2002) Petroleum Reservoir Simulation. Blitzprint Ltd., Calgary, Alberta

Baisch S, Vörös R, Rothert E, Stang H, Jung R (2010) A numerical model for fluid injection induced seismicity at Soultz-sous-Forêts. International Journal of Rock Mechanics & Mining Sciences 47:405–413, https://doi.org/10.1016/j.ijrmms.2009.10.001

Baria R, Michelet S, Baumgaertner J, Dyer B, Gerard A, Nicholls J, Hettkamp T, Teza D, Soma N, Asanuma H, Garnish J, Megel T (2004) Microseismic monitoring of the World's largest potential HDR reservoir. In: Twenty-Ninth Workshop on Geothermal Reservoir Engineering Stanford University, Stanford, California, January 26-28, 2004

Barton C, Zoback M, Moos D (1995) Fluid flow along potentially active faults in crystalline rock. Geology 23:683–686, https://doi.org/10.1130/0091-7613(1995)023<0683:FFAPAF>2.3.CO;2

Berchenko I, Detournay E (1997) Deviation of hydraulic fractures through poroelastic stress changes induced by fluid injection and pumping. International Journal of Rock Mechanics and Mining Sciences 34:1009–1019, https://doi.org/10.1016/S1365-1609(97)80010-X

Bernabé Y (1986) The effective pressure law for permeability in Chelmsford Granite and Barre Granite. International Journal of Rock Mechanics and Mining Sciences & Geomechanics Abstracts 23:267–275, https://doi.org/10.1016/0148-9062(86)90972-1

Biot M (1941) General theory of three-dimensional consolidation. Journal of Applied Physics 12:155–164

Blanpied M, Lockner D, Byerlee J (1995) Frictional slip of granite at hydrothermal conditions. Journal of Geophysical Research 100:13045–13064, doi:10.1029/95JB00862

Boutéca M, Lessi J, Sarda J (1983) Stress changes induced by fluid injection in a porous layer around a wellbore. In: 24th U.S. Symposium on Rock Mechanics June 1983

Brudy M, Zoback M, Fuchs K, Rummel F, Baumgärtner J (1997) Estimation of the complete stress tensor to 8 km depth in the KTB scientific drill holes: Implications for crustal strength. Journal of Geophysical Research 102:18453–18475, https://doi.org/10.1029/96JB02942

Catalli F, Meier M, Wiemer S (2013) The role of Coulomb stress changes for injection-induced seismicity: The Basel enhanced geothermal system. Geophysical Research Letters 40:72–77, doi:10.1029/2012GL054147

Chen J, Jiang F (2015) Designing multi-well layout for enhanced geothermal system to better exploit hot dry rock geothermal energy. Renewable Energy 74:37–48, https://dx.doi.org/10.1016/j.renene.2014.07.056

Chen X, Nakata N, Pennington C, Haffener J, Chang J, He X, Zhan Z, Ni S, Walter J (2017) The Pawnee earthquake as a result of the interplay among injection, faults and foreshocks. Scientific Reports 7, https://doi.org/10.1038/s41598-017-04992-z

Chen Z, Narayan S, Yang Z, Rahman S (2000) An experimental investigation of hydraulic behaviour of fractures and joints in granitic rock. International Journal of Rock Mechanics & Mining Sciences 37:1061–1071, https://doi.org/10.1016/S1365-1609(00)00039-3

Cheng A (1998) On generalized plane strain poroelasticity. International Journal of Rock Mechanics and Mining Sciences 35:183–193, https://doi.org/10.1016/S0148-9062(97)00327-6

Cheng A (2016) Poroelasticity. Springer Nature

Cornet F (2016) Seismic and aseismic motions generated by fluid injections. Geomechanics for Energy and the Environment 5:42–54, http://dx.doi.org/10.1016/j.gete.2015.12.003

Cornet F, Julien P (1989) Stress determination from hydraulic test data and focal mechanisms of induced seismicity. International Journal of Rock Mechanics and Mining Sciences & Geomechanics Abstracts 26:235–248, https://doi.org/10.1016/0148-9062(89)91973-6

Ţene M, Bosma S, Al Kobaisi M, Hajibeygi H (2017) Projection-based Embedded Discrete Fracture Model (pEDFM). Advances in Water Resources 105:205–216, https://doi.org/10.1016/j.advwatres.2017.05.009

Deichmann N, Giardini D (2009) Earthquakes induced by the stimulation of an Enhanced Geothermal System below Basel (Switzerland). Seismological Research Letters 80:784–798, https://doi.org/10.1785/gssrl.80.5.784

Deng K, Liu Y, Harrington R (2016) Poroelastic stress triggering of the December 2013 Crooked Lake, Alberta, induced seismicity sequence. Geophysical Research Letters 43:8482–8491, https://doi.org/10.1002/2016GL070421

Dorbath L, Cuenot N, Genter A, Frogneux M (2009) Seismic response of the fractured and faulted granite of Soultz-sous-Forêts (France) to 5 km deep massive water injections. Geophysical Journal International 177:653–675, https://doi.org/10.1111/j.1365-246X.2009.04030.x

Elbel J, Mack M (1993) Refracturing: Observations and theories. In: SPE Production Operations Symposium, 21-23 March, Oklahoma City, Oklahoma

Evans K, Dahlø T, Roti J (2003) Mechanisms of pore pressure-stress coupling which can adversely affect stress measurements conducted in deep tunnels. Pure and Applied Geophysics 160:1087–1102, https://doi.org/10.1007/PL00012562

Evans K, Genter A, Sausse J (2005a) Permeability creation and damage due to massive fluid injections into granite at 3.5 km at Soultz 1. Borehole observations. Journal of Geophysical Research 110, https://doi.org/10.1029/2004JB003168

Evans K, Moriya H, Niitsuma H, Jones R, Phillips W, Genter A, Sausse J, Jung R, Baria R (2005b) Microseismicity and permeability enhancement of hydrogeologic structures during massive fluid injections into granite at 3 km depth at the Soultz HDR site. Geophysical Journal International 160:388–412, https://doi.org/10.1111/j.1365-246X.2004.02474.x

Evans K, Zappone A, Kraft T, Deichmann N, Moia F (2012) A survey of the induced seismic responses to fluid injection in geothermal and CO_2 reservoirs in Europe. Geothermics 41:30–54, https://doi.org/10.1016/j.geothermics.2011.08.002

Fisher M, Heinze J, Harris C, Davidson B, Wright C, Dunn K (2004) Optimizing horizontal completion techniques in the Barnett Shale using microseismic fracture mapping. In: SPE Annual Technical Conference and Exhibition, 26-29 September, Houston, Texas

Gan Q, Elsworth D (2016) A continuum model for coupled stress and fluid flow in discrete fracture networks. Geomechanics and Geophysics for Geo-Energy and Geo-Resources 2:43–61, https://doi.org/10.1007/s40948-015-0020-0

Gao Q, Cheng Y, Han S, Yan C, Jiang L (2019) Numerical modeling of hydraulic fracture propagation behaviors influenced by pre-existing injection and production wells. Journal of Petroleum Science and Engineering 172:976–987, https://doi.org/10.1016/j.petrol.2018.09.005

Ghassemi A, Tao Q (2016) Thermo-poroelastic effects on reservoir seismicity and permeability change. Geothermics 63:210–224, http://dx.doi.org/10.1016/j.geothermics.2016.02.006

Guglielmi Y, Cappa F, Avouac J, Henry P, Elsworth D (2015) Seismicity triggered by fluid injection-induced aseismic slip. Science 348:1224–1226, https://doi.org/10.1126/science.aab0476

Häring M, Schanz U, Ladner F, Dyer B (2008) Characterisation of the Basel 1 enhanced geothermal system. Geothermics 37:469–495, https://doi.org/10.1016/j.geothermics.2008.06.002

Ishibashi T, Elsworth D, Fang Y, Riviere J, Madara B, Asanuma H, Watanabe N, Marone C (2018) Friction-stability-permeability evolution of a fracture in granite. Water Resources Research 54:9901–9918, https://doi.org/10.1029/2018WR022598

Jacquey A, Urpi L, Cacace M, Blöcher G, Zimmermann G, Scheck-Wenderoth M (2018) Far field poroelastic response of geothermal reservoirs to hydraulic stimulation treatment: Theory and application at the Groß Schönebeck geothermal research facility. International Journal of Rock Mechanics and Mining Sciences 110:316–327, https://doi.org/10.1016/j.ijrmms.2018.08.012

Jupe A, Green A, Wallroth T (1992) Induced microseismicity and reservoir growth at the Fjällbacka Hot Dry Rocks Project, Sweden. International Journal of Rock Mechanics and Mining Sciences & Geomechanics Abstracts 29:343–354

Kim H, Xie L, Min K, Bae S, Stephansson O (2017) Integrated In Situ Stress Estimation By Hydraulic Fracturing, Borehole Observations, And Numerical Analysis At The EXP-1 Borehole In Pohang, Korea. Rock Mechanics and Rock Engineering 50:3141–3155, https://doi.org/10.1007/s00603-017-1284-1

Kim K, Ree J, Kim Y, Kim S, Kang S, Seo W (2018) Assessing whether the 2017 M_w 5.4 Pohang earthquake in South Korea was an induced event. Science 360:1007–1009, https://doi.org/10.1126/science.aat6081

King G, Stein R, Lin J (1994) Static stress changes and the triggering of earthquakes. Bulletin of the Seismological Society of America 84:935–953

Kumar D, Ghassemi A (2019) Multistage hydraulic fracturing of EGS wells with application to FORGE. In: Proceedings, 44th Workshop on Geothermal

Reservoir Engineering, Stanford University, Stanford, California
Kwiatek G, Bohnoff M, Dresen G, Schulze A, Schulte T, Zimmermann G, Huenges E (2008) Microseismicity induced during fluid-injection: A case study from the geothermal site at Groß Schönebeck, North German Basin. Acta Geophysica 58:995–1020, https://doi.org/10.2478/s11600-010-0032-7
Kwiatek G, Bulut F, Bohnhoff M, Dresen G (2014) High-resolution analysis of seismicity induced at Berlín geothermal field, El Salvador. Geothermics 52:98–111, https://dx.doi.org/10.1016/j.geothermics.2013.09.008
Kwiatek G, Saarno T, Ader T, Bluemle F, Bohnhoff M, Chendorain M, Dresen G, Heikkinen P, Kukkonen I, Leary P, Leonhardt M, Malin P, Martínez-Garzón P, Passmore K, Passmore P, Valenzuela S, Wollin C (2019) Controlling fluid-induced seismicity during a 6.1-km-deep geothermal stimulation in Finland. Science Advances 5, https://dx.doi.org/10.1126/sciadv.aav7224
Ladner F, Häring M (2009) Hydraulic characteristics of the Basel 1 Enhanced Geothermal System. Geothermal Resources Council Transactions 33:199–204
McClure M (2015) Generation of large postinjection-induced seismic events by backflow from dead-end faults and fractures. Geophysical Research Letters 42:6647–6654, https://doi.org/10.1002/2015GL065028
McClure M, Horne R (2014) An investigation of stimulation mechanisms in Enhanced Geothermal Systems. International Journal of Rock Mechanics & Mining Sciences 72:242–260, https://doi.org/10.1016/j.ijrmms.2014.07.011
Meier P, Rodríguez A, Bethmann F (2015) Lessons learned from Basel: New EGS projects in Switzerland using multistage stimulation and a probabilistic traffic light system for the reduction of seismic risk. In: Proceedings World Geothermal Congress 2015, Melbourne, Australia
Miller S (2015) Modeling enhanced geothermal systems and the essential nature of large-scale changes in permeability at the onset of slip. Geofluids 15:338–349, https://doi.org/10.1111/gfl.12108
Miller S, Nur A (2000) Permeability as a toggle switch in fluid-controlled crustal processes. Earth and Planetary Science Letters 183:133–146, https://doi.org/10.1016/S0012-821X(00)00263-6
Minner W, Wright C, Stanley G, de Pater C, Gorham T, Eckerfield L, Hejl K (2002) Waterflood and production-induced stress changes dramatically affect hydraulic fracture behavior in Lost Hills infill wells. In: SPE Annual Technical Conference and Exhibition, 29 September - 2 October, San Antonio Texas
Morrow C, Bo-Chong Z, Byerlee J (1986) Effective pressure law for permeability of Westerly Granite under cyclic loading. Journal of Geophysical Research 91:3870–3876, https://doi.org/10.1029/JB091iB03p03870
Norbeck J, McClure M, Horne R (2018) Field observations at the Fenton Hill enhanced geothermal system test site support mixed-mechanism stimulation. Geothermics 74:135–149, https://doi.org/10.1016/j.geothermics.2018.03.003
Oda M (1986) An equivalent continuum model for coupled stress and fluid flow analysis in jointed rock masses. Water Resources Research 22:1845–

1856, https://doi.org/10.1029/WR022i013p01845
Pearson C (1981) The relationship between microseismicity and high pore pressures during hydraulic stimulation experiments in low permeability granitic rocks. Journal of Geophysical Research 86:7855–7864, https://doi.org/10.1029/JB086iB09p07855
Pijnenburg R, Verberne B, Hangx S, Spiers C (2018) Deformation behavior of sandstones from the seismogenic Groningen Gas Field: Role of inelastic versus elastic mechanisms. Journal of Geophysical Research: Solid Earth 123:5532–5558, https://doi.org/10.1029/2018JB015673
Pine R, Batchelor A (1984) Downward migration of shearing in jointed rock during hydraulic injections. International Journal of Rock Mechanics and Mining Sciences & Geomechanics Abstracts 21:249–263, https://doi.org/10.1016/0148-9062(84)92681-0
Rice J, Cleary M (1976) Some basic stress diffusion solutions for fluid-saturated elastic porous media with compressible constituents. Reviews of Geophysics and Space Physics 14:227–241, https://doi.org/10.1029/RG014i002p00227
Robinson E, Potter R, McInteer B, Rowley J, Armstrong D, Mills R (1971) A preliminary study of the nuclear subterrene
Rybach L (2010) "The future of geothermal energy" and its challenges. In: Proceedings World Geothermal Congress 2010, Bali, Indonesia
Schoenball M, Dorbath L, Gaucher E, Wellmann J, Kohl T (2014) Change of stress regime during geothermal reservoir stimulation. Geophysical Research Letters 41:1163–1170, https://doi.org/10.1002/2013GL058514
Segall P (1989) Earthquakes triggered by fluid extraction. Geology 17:942–946, https://doi.org/10.1130/0091-7613(1989)017<0942:ETBFE>2.3.CO;2
Shiozawa S, McClure M (2014) EGS designs with horizontal wells, multiple stages, and proppant. In: Proceedings, Thirty-Ninth Workshop on Geothermal Reservoir Engineering, Stanford, California
Shuck L (1977) Method for selectively orienting induced fractures in subterranean Earth formations. U.S. Patent No. 4005750
Stein R (1999) The role of stress transfer in earthquake occurrence. Nature 402:605–609, https://doi.org/10.1038/45144
Stein S, Wysession M (2003) An Introduction to Seismology, Earthquakes, and Earth Structure. Blackwell Publishing Ltd.
Tester J, Anderson B, Batchelor A, Blackwell D, DiPippo R, Drake E, Garnish J, Livesay B, Moore M, Nichols K, Petty S, Toksöz M, Veatch R (2006) The Future of Geothermal Energy
Townend J, Zoback M (2000) How faulting keeps the crust strong. Geology https://doi.org/10.1130/0091-7613(2000)28<399:HFKTCS>2.0.CO;2
US Department of Energy (2019) The *GeoVision* Roadmap: A Pathway Forward
Vermylen J, Zoback M (2011) Hydraulic fracturing, microseismic magnitudes, and stress evolution in the Barnett Shale, Texas, USA. In: SPE Hydraulic Fracturing Technology Conference, 24-26 January, The Woodlands, Texas, USA

Villeneuve M, Heap M, Kushnir A, Qin T, Baud P, Zhou G, Xu T (2018) Estimating in situ rock mass strength and elastic modulus of granite from the Soultz-sous-forêts geothermal reservoir (France). Geothermal Energy 6, https://doi.org/10.1186/s40517-018-0096-1

Walsh J (1965) The effect of cracks in rocks on poisson's ratio. Journal of Geophysical Research 70:5249–5257, https://doi.org/10.1029/JZ070i002p00381

Wang H (2000) Theory of Linear Poroelasticity with Applications to Geomechanics and Hydrogeology. Princeton Series in Geophysics, Princeton University Press, Princeton, NJ

Warpinski N, Branagan P (1989) Altered-stress fracturing. Journal of Petroleum Technology 41:990–997, https://doi.org/10.2118/17533-PA

Zang A, Oye V, Jousset P, Deichmann N, Gritto R, McGarr A, Majer E, Bruhn D (2014) Analysis of induced seismicity in geothermal reservoirs - An overview. Geothermics 52:6–21, https://dx.doi.org/10.1016/j.geothermics.2014.06.005

Ziagos J, Phillips B, Boyd L, Jelacic A, Stillman G, Hass E (2013) A technology roadmap for strategic development of enhanced geothermal systems. In: Thirty-Eighth Workshop on Geothermal Reservoir Engineering

Zoback M, Harjes H (1997) Injection-induced earthquakes and crustal stress at 9 km depth at the KTB deep drilling site, Germany. Journal of Geophysical Research 102:18477–18491, https://doi.org/10.1029/96JB02814

Zoback M, Healy J (1992) In situ stress measurements to 3.5 km depth in the Cajon Pass Scientific Research Borehole: Implications for the mechanics of crustal faulting. Journal of Geophysical Research 97:5039–5057, https://doi.org/10.1029/91JB02175

Zoback M, Townend J (2001) Implications of hydrostatic pore pressures and high crustal strength for the deformation of intraplate lithosphere. Tectonophysics 336:19–30, https://doi.org/10.1016/S0040-1951(01)00091-9

Zoback M, Townend J, Grollimund B (2002) Steady-state failure equilibrium and deformation of intraplate lithosphere. International Geology Review 44:383–401, https://doi.org/10.2747/0020-6814.44.5.383